Parallel Coupled CFD and CSD Modelling of Steel Tower Response to Blast Loading

Joseph D. Baum[1], Eric L. Mestreau[1], Hong Luo[1], Rainald L? ner[2] and Danielle Pelesonne[3]

[1]Science Applications International Corporation/ACBU,
1710 SAIC Drive, MS 2-6-9, Mclean, VA 22102, USA
E-mail: baumj@saic.com
[2]CSI, George Mason University, Fairfax, VA 22030, USA
[3]Engineering and Software System Solutions, Solana Beach, CA, 92075, USA

Key Words: Parallel Algorithm, Coupled CFD and CSD, Loose coupling, Embedded Algorithms

ABSTRACT

The spate of recent terrorist attacks around the world has increased the need for a coupled Computational Fluid Dynamics (CFD) and Computational Structural Dynamics (CSD) methodology capable of modeling the response of targeted structures to blast loading. Two approaches are used to model fluid/structure interaction. The so called 'tight coupling' approach that requires solving both CFD and CSD as one coupled set of equations, and the 'loose coupling' approach that decouples the CFD and CSD sets of equations and uses projection methods to transfer interface information between the domains. We adopted the latter method, as it allows us to use pre-existing, well-established, validated codes: FEFLO98 for CFD, and variants of DYNA3D for CSD. These variants include General Atomic's GADYNA and ES3's MARS3D. FEFLO98 solves the time-dependent, compressible Euler and Reynolds-Averaged Navier-Stokes equations on an adaptive, unstructured mesh of tetrahedral elements. DYNA3D solves explicitly the large deformation, large strain formulation equations on an unstructured grid composed of bricks and hexahedral elements.

The initial domain coupling of the CFD and CSD methods was based on the so-called "glued-mesh" approach, where the CFD and CSD faces matched identically. Failure of this approach to model severe structural deformations, as well as crack propagation in steel and concrete, led us to the development of the so-called "embedded-mesh" approach, where the CSD objects float through the CFD domain. While each approach has it's own advantages, limitations and deficiencies, the embedded approach has proven to be superior for modeling severe structural deformations under blast and fragment loading.

The Numerical Methodology

The flow solver employed is FEFLO98, a 3-D adaptive, unstructured, edge-based hydro-solver based on the Finite-Element Method Flux-Corrected Transport (FEM-FCT) concept [L? 2]. It solves the Arbitrary Lagrangean-Eulerian (ALE) formulation of the Euler and Reynolds-averaged turbulent, Navier-Stokes equations. The high order scheme used is the consistent-mass Taylor-Galerkin algorithm. Combined with a modified second-order Lapidus artificial viscosity scheme, the resulting scheme is second-order accurate in space, and fourth-order accurate in phase. The spatial mesh adaptation is based on local H-refinement, where the refinement/deletion criterion is a modified H2-seminorm [L? 2] based on a user-specified unknown. Most of the shock wave propagation cases require the use of a blend of density and energy. FEFLO98 supports various equations of states including real air, water, SESAME and JWL with afterburning. Particles can also be used. They are treated as a solid phase, exchanging mass, momentum and energy with the fluid.

The structural dynamics solver is DYNA3D [Wh91], an unstructured, explicit finite element code. DYNA3D is well suited for modeling large deformations and provides a good base for non-linear materials with elasto-plastic compartmental laws with rupture. DYNA3D incorporates a large library of materials and various equations-of-state, as well as many kinematic options, such as slidelines and contacts. Furthermore, DYNA3D is a well proven and benchmarked solver used extensively in the CSD community.

Parallelization Issues: The coupled methodology uses shared memory across O(500) CPU's using open-MP standard. As we typically encounter many partitions (CFD FEM, CFD particles, CSD FEM, CSD contacts, fluid-structure coupling, CTD), while conducting transient problems with large CPU load variations, MPI would have been very expensive for frequent mesh redistribution, adaptation, and remeshing. In addition, as the main focus of our efforts has been maximizing the physical realism, we prefer to optimize the algorithms for the physics of the individual disciplines, maximize the performance on the individual processor, and provide low cache misses, pipelining, and vectorization.

Modeling of terrorist Attack on a steel Tower

Of interest here is one of the more complex simulations conducted: external blast interaction with a multi-chamber, multi-floor bridge-support steel tower. All dimensions and material properties for the compartments, rivets, reinforcements, plates and construction methods were modeled accurately according to industry standards and practices. The structure modeled here is only a small section of a generic steel tower supporting a suspension bridge. Only the section of the tower near the road (five sections above and below road level) was modeled, using appropriate loading boundary conditions on top (weight of upper tower section plus the suspension cable load) and bottom. The ten-segment tower is shown in Figs 1a and 1b. A single level construction is shown in Fig 1c, with an expanded view in Fig 1d showing the accurate modeling of the structure, including all relevant details such as rivets and L-plates.

The modeling assumes a charge located on the roadway near the tower, about the mid-height of ten-section (Fig 2). The distance between the charge and the tower was determined by examining several existing bridges. The numerical methodology models the HE detonation initiation, the detonation wave propagation within the explosive, detonation products diffraction after detonation completion, blast load interaction with the structure, structural deformation, steel panel fragmentation and blast load diffraction between the accelerating fragments to load the next layer of steel panels. Figure 2 shows pressure contours just as the blast impacts the steel tower, very shortly after detonation completion.

Figures 2b and 2c show a very interesting process, not often observed in blast-structure interaction modeling. The figure shows pressure contours on the X-Y plane (plan view) and the X-Z plane (side view). Plane definitions are shown in Fig 2a. Typically, one would expect to see a shock wave reflection from the impacted surface. However, in this case, because the surface failed so soon after blast wave impact, the resulting rarefaction wave caught up with the reflecting shock and eliminated it completely. The side view (Fig 2c) shows some weak reflections above and below the blast plane, as blast pressure amplitude weakens, and the surface does not fail as fast or move so fast (hence, a weaker rarefaction) as on the blast plane.

The structural velocity and pressure (the pressure experienced by the structure) results at =0.3 ms (Figs 2) show that the elongated charge sheared the front faces nearest the charge for six out of the eight cells. The extreme two cells that experience lower pressure loads fail too, though in a bending mode. In this simulation we decided not the model crack propagation in the steel panel, a rather CPU expensive process, but rather generate a single fragment from each element that fails. To compute the actual crack propagation in the steel would require significantly finer resolution than intended for this preliminary study.

Figures 3a and 3b show CSD pressure contours on the X-Z planes at t=0.3 ms and t=0.8 ms, after removing the near half of the structure. Figure 3a shows significant pressure loading on the second layer of cell faces, and the resulting significant structural velocity in response to the high-pressure loading. This is a typical response to loading from large HE charges. For smaller

charges, or for larger charges later on in the computations (after further expansion of the blast and peak-pressure reduction) we will observe lower pressure loading which by themselves would not result in structural failure. In these cases, failure often results from the impact of high-velocity fragments, generated by the failure of an upstream steel panel. At t=0.8 ms. Fig 3b shows the high pressure loading on the central cell of the third layer. Notice that the high pressure by itself did not fail the panel, at least at this time. Yet, fragments generated by the failure of the first and second layers ar puncturing this layer. Also note the while at this time we observe that on the plane of the charge the pressure already reached the third layer of cell, but above and bellow the blast still deforms the second layer.

Examination of the results at t=2.5 ms shows that although the maximum airblast pressure has been reduced by this time, a significant amount of kinetic energy is still contained in the moving structure and fragments, with the maximum fragment velocity of about 1200 m/sec.

Figures 4a show the complete surface at t=2.72 ms. At this time, the pressure contours results show that the peak pressure of the incident blast leading penetration into the structure has been reduced to a level that does not shear the steel instantaneously. Rather, we now observe some reflection from surfaces that take longer to fail, and thus produced pressure reflection. At this time the cut views of structure pressure and velocity show incident pressure reduction such that the last cell on the charge level does not fail due to pressure alone (though it responds with a lower velocity). This cell will fail later due to the high velocity steel fragment impact.

Finally, Figs 4b and 4c show front and rear views of the tower at 6.0 ms. The results show that for this charge, most walls at the center-level were breached, resulting in tower buckling under the pressure of the rest of the tower above and the bridge suspension cables.

REFERENCES

R. Löhner and J.D. Baum (2003) "Adaptive H-Refinement on 3-D Unstructured Grids for Transient Problems", Int. J. Num. Meth. Fluids 14, 1407-1419.
R.G. Whirley and J.O. Hallquist (1982) "DYNA3D, A Nonlinear Explicit, Three-Dimensional Finite Element Code for Solid and Structural Mechanics - User Manual" UCRL-MA-107254 (1991), also Comp. Meth. Appl. Mech. Eng. 33, 725-757.

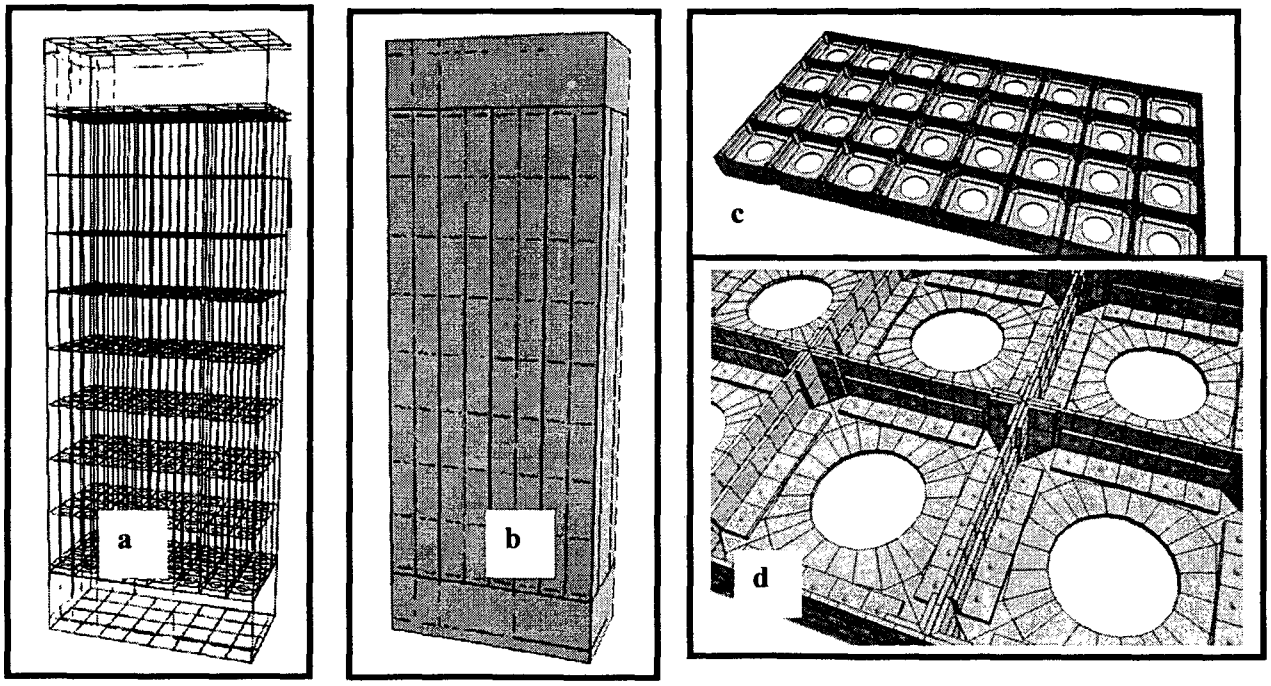

Fig. 1. The ten level steel tower with expanded views of one level of the structure, and the CSD mesh showing the shell elements and the rivets.

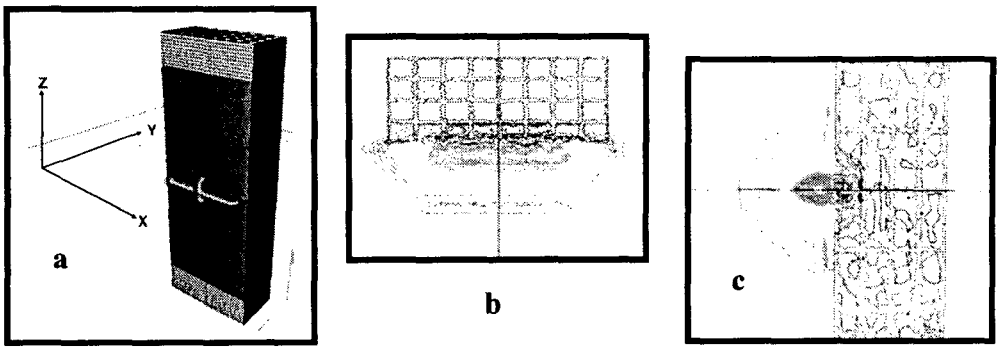

Fig. 2a. Initial positioning of the elongated charge in front of the steel tower at road level. Figs. 2b and 2c. Blast wave diffraction about the deforming structure at t=0.3 ms. Notice: no reflection from the fast-shearing front plates.

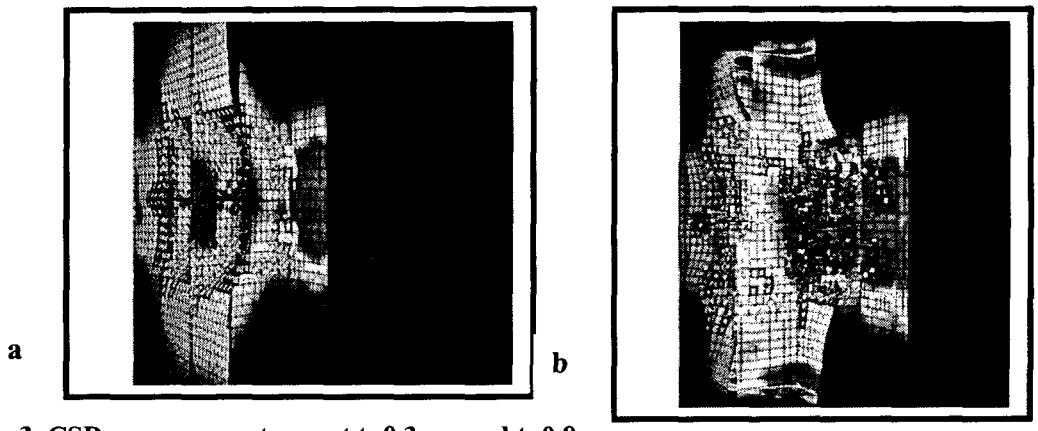

Fig. 3. CSD pressure contours at t=0.3 ms and t=0.8 ms.

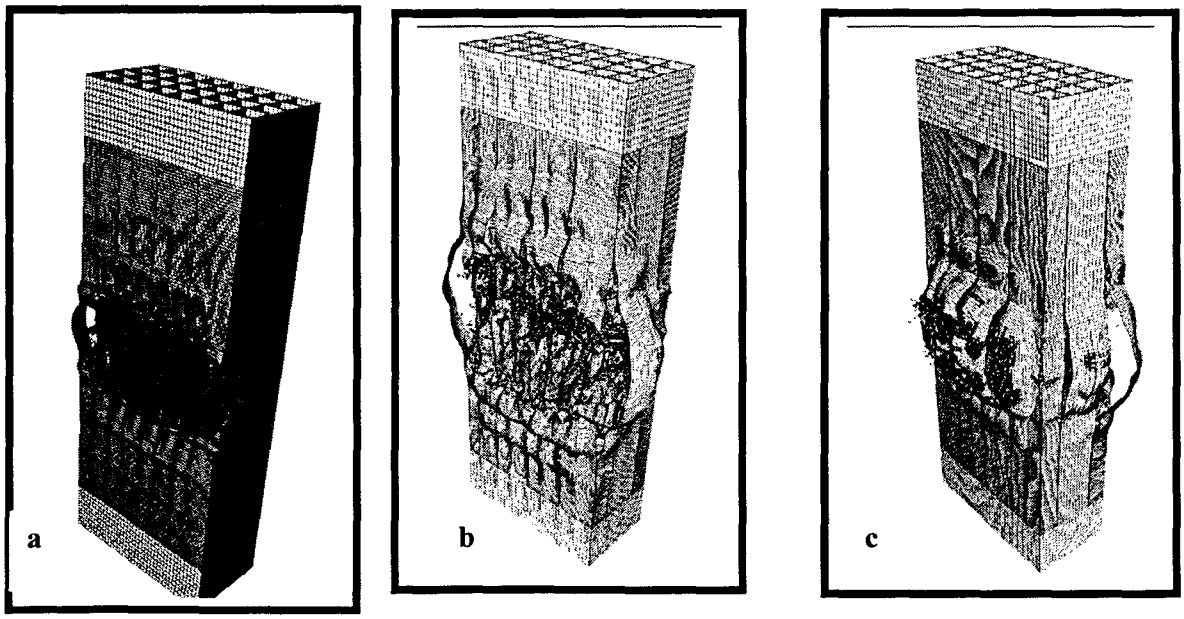

Fig. 4. Structural surface at t=2.72 ms and front and rear views of the surface at 6.0 ms showing complete structural failure at the charge level. The tower would collapse under the load of the top portion and the suspension bridge steel cables.